

Dislocation nucleation from near surface void under static tensile stress in Cu

A. S. Pohjonen,^{1,a)} F. Djurabekova,¹ K. Nordlund,¹ A. Kuronen,¹ and S. P. Fitzgerald²

¹*Helsinki Institute of Physics and the Department of Physics, Accelerator Laboratory,
P. O. Box 43, FIN-00014 University of Helsinki, Helsinki, Finland*

²*EURATOM/CCFE Fusion Association, Culham Science Centre, Abingdon OX14 3DB, United Kingdom*

(Received 14 December 2010; accepted 4 June 2011; published online 21 July 2011)

We examine a possible mechanism for the formation of protrusions on a metallic surface held in a sufficiently high electric field in the presence of a near-surface void. By means of molecular dynamics simulations we show that the high tensile stress exerted on a Cu {110} surface with a near-surface void can promote the nucleation of dislocations on the void surface. These dislocations cause slip along {111} crystallographic planes leading to mass transport in the volume above the void. We find a linear correlation between the radius of the void and the maximum depth for the growth to occur. © 2011 American Institute of Physics. [doi:10.1063/1.3606582]

I. INTRODUCTION

Dislocations are involved in multiple mechanisms causing deformation of crystalline material under stress. If a dislocation source is located near the surface, the application of stress will lead to topological modification of the surface. For example, the multiplication of dislocations via a Frank-Read source can cause dramatic deformation of the crystal as a result of dislocation glide.^{1,2} The phenomenon of whisker growth on a metal surface was proposed to be explained by the activation of Bardeen-Herring source of dislocations.^{3,4} However, the efficacy of such a source relies on long-time diffusion processes since it acts via climb mechanism. Dislocations are also known to nucleate on stress concentrators, such as voids and inclusions under stress.^{1,5} In the presence of a nearby surface, the dislocations are strongly attracted to the surface by the so-called image-force which appears due to surface stress relief.

If a metal surface is subjected to a sufficiently high electric field ($>\sim 100$ MV/m), it experiences a constant tensile stress exerted on the partially charged surface atoms via the Lorentz force.⁶ Since dislocations are activated by applied stress, they can cause modification of the surface under this electric-field-induced stress. It has been suggested⁷ that the significant enhancement of electric field observed⁸ prior to the vacuum arcing phenomenon⁹ over a metal surface exposed to a sufficiently high electric field is related to topological modifications on the surface. Hence dislocation processes may be involved in the triggering of the vacuum arcing in such a condition.

The performance of accelerating structures in linear colliders is severely limited by the fact that the electrical breakdown rate (BDR)—the probability of vacuum arcing—becomes non-negligible at some critical electric field strength, significantly lower than that at which the failure of the metal surface is expected.^{10,11} The problem has attracted renewed interest since the BDR is one of the critical factors limiting the performance of the Compact Linear Collider currently

under development at CERN.¹⁰ Also, the design of the ITER fusion reactor will be modified to involve an all-tungsten divertor,¹² and material erosion due to electric arcs has been recognized to be of comparable magnitude in tungsten as the erosion due to sputtering.¹³ However, there is still no clear understanding of the main cause of vacuum arcs (electrical breakdowns), nor a definite scenario of metal surface evolution processes that can result in the destructive arcing phenomenon. Experiments clearly show that there are random spots on metal surfaces releasing high currents of electrons prior to a vacuum arcing discharge,⁷ which are presumed to originate from locally enhanced fields. However, the questions, what causes this enhancement and how the surface evolves under the electric field, are still open.

In this work, we describe observations of a dislocation nucleation mechanism on a near-surface void under tensile stress exerted on the surface in molecular dynamics (MD) simulations. Dislocation nucleation^{14–16} and dislocation nucleation on voids^{5,17–23} have been studied earlier. Some studies were done with the use of the MD technique. Rudd and Belak and Rudd *et al.* have observed prismatic loops generated at the void surface under stress transporting material away from the void.^{18,19} Seppala *et al.* have investigated the effect of stress triaxiality on void growth due to dislocations²⁰ and void coalescence.²¹ Marian *et al.* observed nanovoid deformation in aluminum through dislocation emission.²² Recently Bringa *et al.* observed shear loop nucleation on voids in copper.²³ Dislocation nucleation dependence on strain rate has been examined by Spearot *et al.*¹⁶ and Zhu *et al.*¹⁵

In our simulations, we assume the presence of a near-surface void. The presence of such voids can be explained by the Kirkendall effect due to the oxidation of the surface.^{24,25} Also, voids can be formed due to the technological imperfection of the metal production or electromigration.²⁶ Hence, we formulate the following hypothesis: tensile stress exerted on a metal surface with a near surface void can cause mass transport in the volume located above the void. This mass transport is carried by the dislocations nucleated at the void⁵ due to the shear stress which appears in the direction from the void to the surface. The mass transport then leads to

^{a)}Electronic mail: aarne.pohjonen@iki.fi.

the growth of a microscopic protrusion, which in turn will cause a field enhancement. We tested this hypothesis by performing molecular dynamics simulations,²⁷ which can provide an atomistically accurate picture of dislocation nucleation. After the simulation we analyzed the frames of the simulated box by the centrosymmetry analysis¹⁴ to investigate the formation of stacking faults and dislocations.

II. ORIGIN OF TENSILE STRESS EXERTED ON METAL SURFACE

In our simulations, we focus on a single metal surface exposed to the external electric field. According to Gauss law, a conducting surface in the presence of an electric field becomes charged with the surface charge density $\sigma_s = \epsilon_0 |\vec{E}|$, where \vec{E} is the field near the surface.²⁸

If the surface is perfectly flat, the local field is the same as the external field \vec{E}_0 and the charge of the surface is $q_s = \sigma_s A$, where A is the area of the surface. If so, the charged surface experiences the Lorentz force

$$\vec{F}_L = \sigma A \vec{E}, \quad (1)$$

which is aligned along the field. Since this force is the product of the charge and the field, it is always directed outwards from the surface. Thus we can obtain the tensile stress exerted on a conducting surface in the presence of an electric field by dividing the Lorentz force (1) with the area A of the surface.

$$T_{zz} \hat{n} = \vec{F}_L / A = \sigma \vec{E}_0 = \epsilon_0 |\vec{E}_0|^2 \hat{n}, \quad (2)$$

where \hat{n} is the unit vector normal to the surface. This equation allows for an estimation of the stress exerted on a conducting surface by an electric field. The critical field, which causes the breakage of a Cu surface, is known from experiments⁸ to be ~ 10 – 11 GV/m. In this case, the maximal tensile stress becomes $T_{zz} = 0.9$ – 1.1 GPa, which is a significant value, although not sufficient for studying dislocation nucleation within molecular dynamics timespan. Hence we exaggerated the exerted tensile stress in order to be able to study the dislocation mechanisms by MD methods, ranging it between 2.4 and 4.58 GPa, which corresponds to the fields between 16 and 22.7 GV/m.

It must be mentioned that the operational fields for Cu surfaces in the corresponding experiments are about 200 MV/m, however, in the same experiments the enhancement factor of local fields compared to an external field had never been measured below 15.⁸

III. SIMULATIONS

The present simulations were done using the parcas classical MD code.²⁹ Cu was modeled using the Sabochick-Lam interatomic potential,³⁰ well tested with respect to melting and point defect properties.³¹ In order to examine our conclusions on the dislocation mechanism, we also applied the Mishin *et al.* potential,³² developed for the improved description of the elastic and plastic properties of Cu. Both potentials yielded qualitatively similar results. A simulation

cell with a $\{110\}$ surface crystal plane (i.e., the z direction corresponding to one of the $\langle 110 \rangle$ crystal directions) was constructed, with $\langle 111 \rangle$ and $\langle 211 \rangle$ crystal directions in the x and y directions. Periodic boundary conditions were applied in the x and y directions. The three bottom layers of atoms were fixed to prevent any possible drift of the cell, the top layer is open to form a surface. The size of the simulation cell was $S_x = 179$, $S_y = 190$, and $S_z = 194$ Å. Also a set of simulations with different boundary conditions was performed to check that the results remain the same as with periodic boundaries. In these simulations the atoms which form the sides of the simulated cell (the lateral boundaries) were allowed to move only in the z -direction, while the x and y coordinates were fixed.

The simulation cell was relaxed at first without the field for 20 ps and after that a linearly-increasing force was applied to atoms that initially formed the two top atom layers in the time interval 20...120 ps. In our simulations we assigned the force given by Eq. (1) over two top layers of atoms. The ramping of the force was done to avoid the non-equilibrium distribution of the stress throughout the simulation box (such as artificial pressure waves that would be reflected from the fixed bottom layers). In the rest of the simulation the maximal force corresponding to the desired stress was exerted on the same atoms, regardless of their actual position. This approximation is valid until a visible protrusion appears on the surface. Such a protrusion will distort the electric field, locally changing the direction and the absolute value of the force acting on surface atoms. This will result in redistribution of the tensile stress. From this point on, a different simulation technique which takes into account the dynamic evolution of the surface stress should be applied. The temperature of the system was 600 K during the whole simulation. A schematic of the simulation cell with the initial structure is shown in Fig. 1.

In order to introduce the desired tensile stress, the Lorentz force acting on the entire surface is divided between the surface atoms as $\vec{F}_{at} = \vec{F}_L / N_{at}$ where N_{at} is the number of surface atoms.

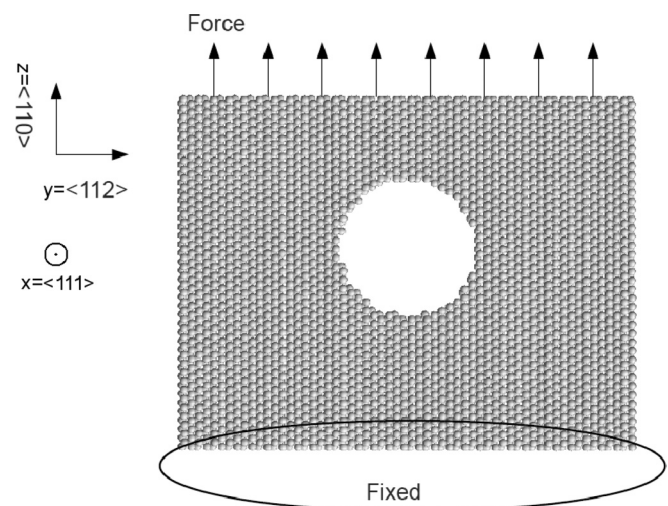


FIG. 1. Schematic of the simulation cell. The force was applied on two top layers of atoms. The three layers of atoms on the bottom were held fixed.

To give a quantitative description of the dislocation nucleation we considered a parameter which characterizes the critical depth at which a dislocation can be emitted within the MD timespan. This parameter exhibited a strong dependence on the radius of the void, temperature and applied stress. The simulations were performed as follows: a spherical void with radius r was systematically placed at different depths H with the interval of 2 Å. The force applied uniformly to the surface atoms pulls the atoms located above the void, causing them to move upwards. The shallow voids are quickly destroyed by this force. The deeper the void, the weaker the atoms are pulled on average. At some depth a dislocation that causes growth of an atomic step on the surface above the void is not emitted during the simulation time. This depth was defined as the critical depth H_{\max} . Since the void was placed in 2 Å intervals, the uncertainty of the observed value of H_{\max} is 1 Å. The procedure was repeated for various values of the void radius r . A similar procedure was repeated for different values of stresses and for the Mishin potential but the interval was different in some cases. For stresses of 2.40 GPa the interval was 10 Å and for the Mishin potential the interval was 5 Å. Due to the Poisson effect, the system strained in the z direction is expected to shrink in the lateral direction. As a matter of fact, this shrinkage can be estimated in the approximation of an isotropic material as follows. If we take as an example the tensile stress of $T_{zz} = 4.58$ GPa, the strain in the z direction in our MD cell is then $\epsilon_{zz} = 0.0115$. Taking into account the Poisson ratio $\nu = 0.34$, the cell should shrink in the lateral direction by $\epsilon_{xx} = \epsilon_{yy} \approx -0.34\epsilon_{zz} = -0.0039$ on average, compensating the lateral compressive stress. However, in our simulation we neglect this phenomenon because in the experiments corresponding to our simulation, the area affected by the field is negligibly small, ~ 0.5 mm², compared to the few cm² size of unaffected surface. This situation will provide only negligible relaxation in the lateral direction of the cell, thus motivating the choice of our boundary conditions.

IV. RESULTS AND DISCUSSION

Snapshots of a simulation with void radius $r = 28$ Å are presented in Fig. 2. Here we show only the atoms on the surfaces and stacking faults, the others being filtered out by the centrosymmetry parameter.¹⁴ It is clearly seen that the nucleation of partial dislocations causes the formation of a protrusion on the surface.

Due to the resolved shear stress acting along $\{111\}$ planes, which are not perpendicular to the surface, we first observe stacking faults in our simulation box along these planes. They do not contribute to the surface protrusion formation directly. However, they do promote the formation of slip along the vertical $\{111\}$ planes by forming steps on the void surface that act as nucleation centers for dislocations. This conclusion is confirmed by examining Fig. 3(a), where the final protrusion is depicted. As can be seen, the shape of the protrusion is a parallelogram with small corner angles of 71°, which corresponds to the angle between two $\{111\}$ planes, perpendicular to the $\{110\}$ surface. The observed stacking faults and the shape of the protrusion show that the dislocations are partials having $1/6 \langle 112 \rangle$ Burgers vectors. These results are presented in Figs. 2 and 3(a). This mechanism is similar to the punching of prismatic loops on an inclusion.^{1,33} If the dislocation emitted in the direction perpendicular to the surface strikes a sideward stacking fault, the dislocation interaction in this case can block the mass transport toward the surface.

The shape of the protrusion formed on the surface together with the observed stacking faults that are created by dislocations moving perpendicular to the surface show that the mechanism is similar to the observations of Rudd and Belak and Rudd *et al.*^{18,19} of the nucleation of prismatic loops. The observation of the stacking faults created by dislocations moving in diagonal directions away from the void is similar to the recent observations of Bringa *et al.*²³ of shear loop nucleation on voids under stress deep in the bulk.

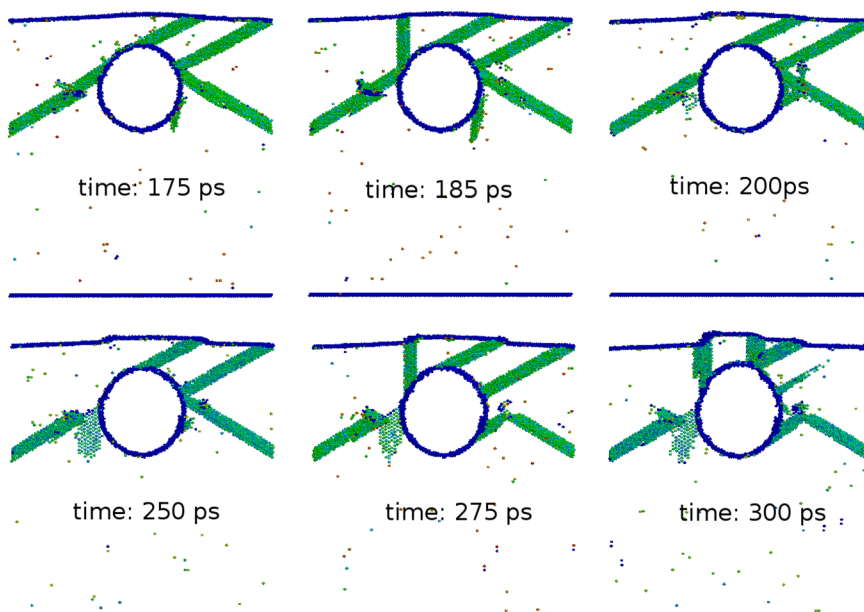


FIG. 2. (Color online) Snapshots of the simulation of the void with radius $r = 28$ Å; temperature of the cell 600 K; applied stress 4.58 GPa. The forces were exerted on atoms on the two top layers. Atoms on the stacking faults and surfaces are shown.

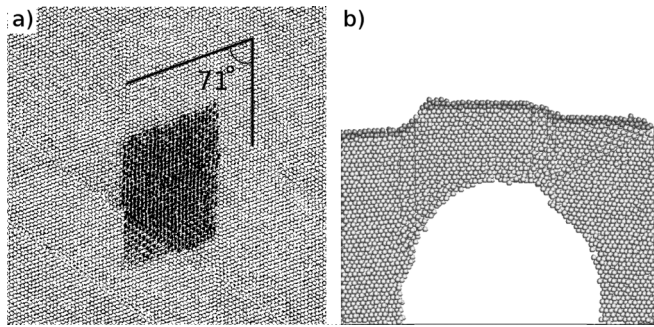


FIG. 3. (a) The surface viewed from above after the dislocations have been nucleated. The gray scale shade of each atom is chosen according to its height, showing a protrusion on the surface that has corners with 71° angles. This shows that the dislocation lines are oriented in $\langle 112 \rangle$ directions and glide on $\{111\}$ planes. (b) Side view of the surface after the protrusion has grown.

The simulation results summarizing the critical depth dependence on void radius in Figs. 4(a) and 4(b) (Sabochnik-Lam potential) and 4(c) (Mishin *et al.* potential) show a linear relation, hence the following criterion for growth of the void can be stated: Growth will occur at a given temperature and time if the inequality (3) holds.

$$H < H_{\max} = a(r - r_0). \quad (3)$$

The simulation results and the size dependence of H_{\max} on the void radius can be understood qualitatively based on the following consideration. The force applied to the surface above the void acts evenly on every atom on the surface. If the structure were perfect, the same stress would be evenly applied to all the atoms. The presence of a void right below the surface violates the uniformity of the stress, for the atoms

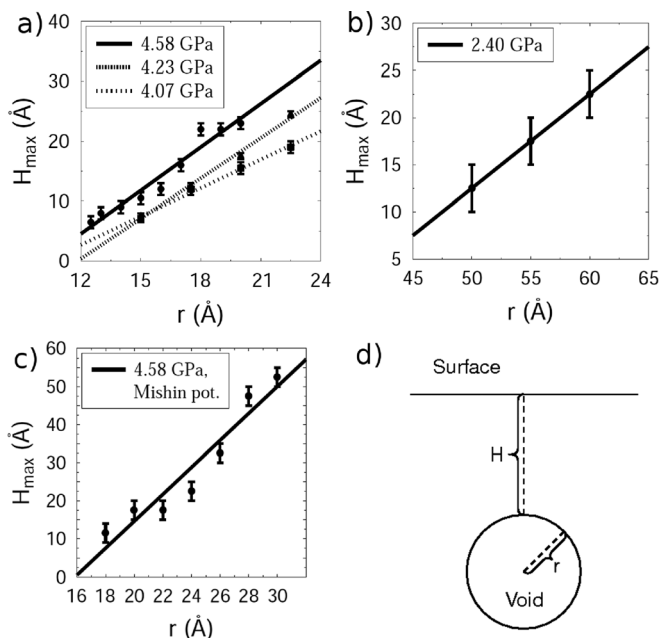


FIG. 4. The dependence of the critical depth H_{\max} on the void radius r in simulations with different stresses using Sabochnik-Lam potential (a) and (b) and Mishin potential (c). A line was fitted to the data by the method of least squares. (d) Schematic of the variables used in systematic set of simulations.

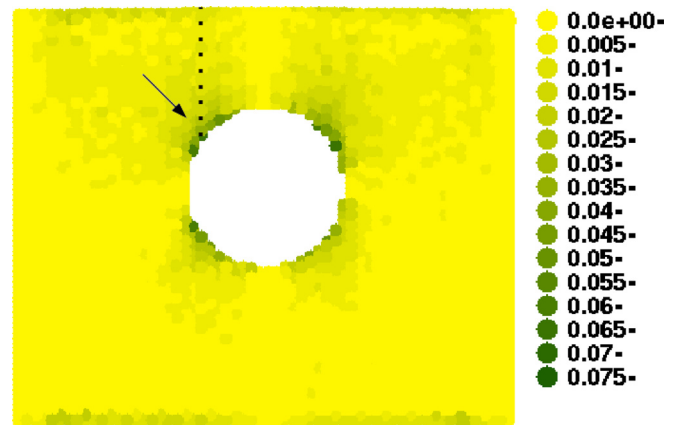


FIG. 5. (Color online) Absolute values of ϵ_{zx} strain component near the void. This is the strain component related to the shear stress on slip plane. The strain was further analyzed along the path that starts at the most strained point on void surface that is shown by the arrow. The path is marked with a dashed line on the figure.

above the ceiling of the void will experience less z -directional tensile stress, T_{zz} , since they are bound to the cell only via the sideways bonds and surface tension. This difference generates a shear stress sufficient to nucleate a dislocation. With the increase of tensile stress on the surface, the shear stress exerted on the atoms connecting the ceiling of the void to the rest of the crystal is growing.

To understand the effect of void size on the dislocation nucleation, we have analyzed the strain of the system as a response to the tensile stress on surface. The strain is related to the stress through the constitutive equation of elasticity,² and therefore the analysis of strain allows us to understand the stress that causes the dislocation to nucleate. To analyze the strain near the void, we have used the software called Open Visualization Tool, OVITO,³⁴ to calculate shear strain components at atom positions in two different cases. Voids with two different radii ($r = 12.5 \text{ \AA}$ and $r = 20 \text{ \AA}$) were placed at the same depth ($H = 24 \text{ \AA}$) below the surface. The stress on surface was ramped to 4.58 GPa in the similar manner as described earlier. The system was initially in 300 K and was cooled after 120 ps to 0 K using the Berendsen temperature control.³⁵ OVITO was used to calculate the zx and zy components of the strain, ϵ_{zx} and ϵ_{zy} , when the system had been cooled to 0 K. The strain field was further analyzed along the line that started at the most strained point on void surface and ended to the surface of the material, as marked with dashed line in Fig. 5. The values of ϵ_{zx} and ϵ_{zy} for the smaller and larger voids are compared in Fig. 6 as a function of the z -coordinate. It is clear that the ϵ_{zx} component of strain is larger on the surface of the larger void, hence, the shear stress on the surface of the larger void is also larger. Because the shear stress on the slip plane is the driving force to activate a dislocation, this result explains why a dislocation is more easily nucleated on the surface of a larger void.

The temperature dependence of the critical depth H_{\max} of a void with radius $r = 18 \text{ \AA}$ was examined by a systematic set of simulations (Fig. 7). The fact that the critical depth has temperature dependence is consistent with dislocation nucleation being thermally activated below the athermal threshold.³⁶

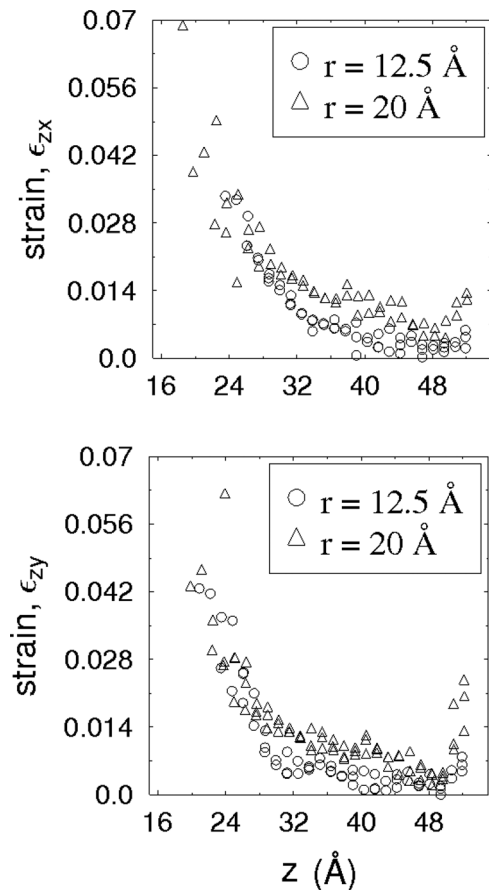


FIG. 6. The strain components ϵ_{zx} and ϵ_{zy} as a function of the z -coordinate of the atom. The atoms were analyzed along the path that starts at the most strained point on void surface and ends to the flat surface of the material, as depicted in Fig. 5 for ϵ_{zx} component. The void surface is at the lower end of the z coordinate value (18.24 Å).

The mechanism presented here can initiate the growth of features on the surface. The longer timescales could in principle cause growth from voids lying deeper beneath the surface, but systematic studies will be required to determine to what extent. We also note that in reality, once a sharp feature has started growing, the electric field over it would be enhanced,³⁷ further increasing the growth.

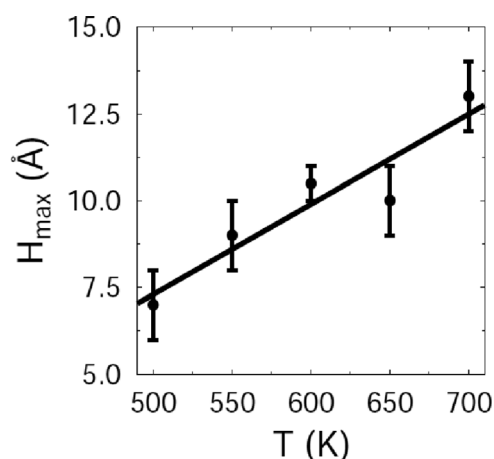


FIG. 7. The critical depth H_{\max} of a void with radius $r = 18$ Å at different temperatures T . In these simulations the Sabochick-Lam potential was used. The applied stress was 4.58 GPa and the simulation time was 420 ps.

V. CONCLUSIONS

In the present work, we showed that dislocations can nucleate on a near-surface void under a constant tensile stress exerted on the surface. This mechanism can eventually lead to the formation of a stable protrusion, or be responsible for a dramatic change in the surface topology. Our result showing that the critical depth depends on temperature is consistent with the stochastic nature of the dislocation nucleation process.^{15,36} Consequently, the events observed under high stress could happen under lower stress over a longer time period. We also observed a criterion for void growth which describes the linear relationship between the critical depth and the radius of the void. The mechanism of dislocation nucleation on a void under tensile stress can be responsible for plasma onset near metal surfaces operated at high electric fields.

ACKNOWLEDGMENTS

We gratefully acknowledge the help from M.Sc Helga Timko in describing results obtained from the experimental DC setup at CERN. The authors acknowledge the assistance of the Finnish IT Center for Science CSC. The research leading to these results has received funding from the European Commission under the FP7 Research Infrastructures project EuCARD, Grant No.227579 and the Finnish Centre of Excellence in Computational Molecular Science (CMS), financed by The Academy of Finland and the University of Helsinki. This work, supported by the European Communities under the contract of Association between EURATOM and CCFE, was carried out within the framework of the European Fusion Development Agreement. The views and opinions expressed herein do not necessarily reflect those of the European Commission. This work was also part-funded by the RCUK Energy Programme under grant EP/I501045.

¹D. Hull and D. J. Bacon, *Introduction to Dislocations* (Butterworth Heinemann, 2001).

²J. P. Hirth and J. Lothe, *Theory of Dislocations* (Krieger, Malabar, Florida, 1992), 2nd ed.

³J. Eshelby, *Phys. Rev.* **91**, 755 (1953).

⁴B. Lee and D. Lee, *Acta Materialia* **46**, 3701 (1998).

⁵D. C. Ahn, P. Sofronis, M. Kumar, J. Belak, and R. Minich, *J. Appl. Phys.* **101**, 063514 (2007).

⁶F. Djurabekova, S. Parviainen, K. Nordlund, and A. Pohjonen, *Phys. Rev. E* (2010), submitted for publication.

⁷R. Boxman, *Handbook of Vacuum Arc Science and Technology* (Noyes Publications, 1995).

⁸A. Descoedres, Y. Levinsen, S. Calatroni, M. Taborelli, and W. Wuensch, *Phys. Rev. ST Accel. Beams* **12**, 092001 (2009).

⁹R. Behrisch, in *Physics of Plasma-Wall Interactions in Controlled Fusion*, edited by D. E. Post and R. Behrisch (Plenum Press, New York, 1986), Vol. 131 of NATO ASI Series, Series B: Physics, pp. 495-513.

¹⁰W. Wuensch, *AIP Conf. Proc.* **877**, 15 (2006).

¹¹A. Descoedres, T. Ramsvik, S. Calatroni, M. Taborelli, and W. Wuensch, *Phys. Rev. ST Accel. Beams* **12**, 032001 (2009).

¹²N. Holtkamp, *Fusion Engineering and Design* **84**, 98 (2009).

¹³V. Rohde, *Arc Surface Damage in Fusion Reactors*, Breakdown Physics Workshop, 6-7.5 at CERN (2010).

¹⁴J. Knap and M. Ortiz, *Phys. Rev. Lett.* **90**, 226102 (2003).

¹⁵T. Zhu, J. Li, A. Samanta, A. Leach, and K. Gall, *Phys. Rev. Lett.* **100**, 025502 (2008).

¹⁶D. Spearot, M. Tschopp, and D. McDowell, *Scripta Materialia* **60**, 675 (2009).

¹⁷D. C. Ahn, P. Sofronis, and R. Minich, *J. Mech. Phys. Solids* **54**, 735 (2006).

- ¹⁸E. Rudd and J. Belak, *Comput. Mat. Sci.* **24**, 148 (2002).
- ¹⁹R. Rudd, E. Seppala, L. Dupuy, and J. Belak, *Journal of Computer-Aided Materials Design* **14**, 425 (2007).
- ²⁰E. Seppala, J. Belak, and R. Rudd, *Phys. Rev. B* **69**, 134101 (2004).
- ²¹E. Seppala, J. Belak, and R. Rudd, *Phys. Rev. Lett.* **93**, 245503 (2004).
- ²²J. Marian, J. Knap, and M. Ortiz, *Acta Materialia* **53**, 2893 (2005).
- ²³E. Bringa, S. Traiviratana, and M. Meyers, *Acta Materialia* **58**, 4458 (2010).
- ²⁴B. Selikson, *Proceedings of the IEEE* **57**, 1594 (1969).
- ²⁵H. J. Lee and J. Yu, *J. Electron. Mater.* **37**, 1102 (2008).
- ²⁶G. Schneider, G. Denbeaux, E. H. Anderson, B. Bates, A. Pearson, M. A. Meyer, E. Zschech, D. Hambach, and E. A. Stach, *Appl. Phys. Lett.* **81**, 2535 (2002), URL <http://link.aip.org/link/?APL/81/2535/1>.
- ²⁷M. P. Allen and D. J. Tildesley, *Computer Simulation of Liquids* (Oxford Science Publications, 1989).
- ²⁸J. R. Reitz, F. J. Milford, and R. W. Christy, *Foundations of Electromagnetic Theory* (Addison-Wesley Publishing company, 1993).
- ²⁹K. Nordlund, PARCAS computer code (2007).
- ³⁰M. J. Sabochick and N. Q. Lam, *Phys. Rev. B* **43**, 5243 (1991).
- ³¹K. Nordlund and R. S. Averback, *Phys. Rev. Lett.* **80**, 4201 (1998).
- ³²Y. Mishin, M. J. Mehl, D. A. Papaconstantopoulos, A. F. Voter, and J. D. Kress, *Phys. Rev. B* **63**, 224106 (2001).
- ³³V. V. Bulatov, W. G. Wolfer, and M. Kumar, *Scripta Materialia* **63**, 144 (2010).
- ³⁴A. Stukowski, *Modelling Simul. Mater. Sci. Eng.* **18**, 015012 (2010).
- ³⁵H. J. C. Berendsen, J. P. M. Postma, W. F. van Gunsteren, A. DiNola, and J. R. Haak, *J. Chem. Phys.* **81**, 3684 (1984).
- ³⁶J. Li, *MRS Bulletin* **32**, 151 (2007).
- ³⁷C. J. Edgcombe and U. Valdre, *J. Microscopy* **203**, 188 (2001).